Int. J. Heat Mass Transfer. Vol. 36, No. 14, pp. 3437–3448, 1993
Printed in Great Britain

0017–9310/93 $6.00+0.00

Mass and momentum transport in smooth falling liquid films laminarized at relatively high Reynolds numbers

ISSAM MUDAWAR† and RONALD A. HOUPT

Boiling and Two-Phase Flow Laboratory, School of Mechanical Engineering, Purdue University, West Lafayette, IN 47907, U.S.A.

(*Received* 24 *August* 1992 *and in final form* 11 *February* 1993)

Abstract—One and two component velocity measurements were made in smooth laminar falling liquid films formed on the exterior of a vertical column using laser-Doppler velocimetry (LDV). Solutions of water and propylene glycol were used to create thick films and allow room for relatively large traverses of the measuring probe volume. These viscous solutions yielded smooth laminar films at Reynolds numbers as high as 4997, contrary to commonly accepted criteria for transition between falling film regimes. Measurement of the Reynolds stress verified that these films were indeed laminar. Modeling was performed via the integral momentum approach adapted to cylindrical coordinates with the assumption of a velocity profile preserved along the film development region. Velocity predictions varied from experimental results by less than 12.5% while film thickness predictions were within 8.7%.

1. INTRODUCTION

CONDENSERS, evaporators, distillation columns, chemical reactors, and nuclear reactor cores are all important examples of applications demanding a good understanding of falling liquid film hydrodynamics. Despite decades of research on this topic, practical engineering still relies upon simplistic approaches to predicting the transport characteristics of films. An example of this is the fairly common practice of grouping falling liquid films into different regimes based solely upon the film Reynolds, $Re = 4\Gamma/\mu$. One commonly accepted grouping is [1]: *laminar* for $Re < 33$, *wavy laminar* for $33 < Re < 1600$, and *turbulent* for $Re > 1600$.

While this grouping seems to yield fair approximations in many instances, several exceptions can be cited. Wilkes and Nedderman [2] reported that adding surface active agents to a liquid could suppress waves, indicating that the flow regimes are not uniquely dependent upon Reynolds number. Despite reducing the effectiveness of film transport, this suppression of waves can yield a more predictable film behavior which is important to processes such as glass making and those involving temperature sensitive and volatile fluids. Portalski [3] found agreement with their results. Ho and Hummel [4] reported evidence of transition to turbulence just beginning to occur at a Reynolds number of 2810. Cook and Clark [5] discussed the possibility that a length of smooth laminar flow may be followed immediately downstream by a region of wavy flow, therefore a flow surface could be too short to allow waves to form. Furthermore, they made velocity measurements in 'ripple free' films over a Reynolds number range of 308 to 980. Nakoryakov *et al.* [6] reported smooth films for Reynolds numbers varying from 32 to 120. Yet another team, Semena and Mel'nichuk [7], noted that their experimentally measured velocities were higher than those predicted from laminar theory, but agreement improved as the Reynolds number was *increased* from 270 to 1640. They also concluded that none of their films were turbulent. Other related issues pertaining to liquid film stability can be found elsewhere [8, 9].

Since measuring the velocity field in a falling liquid film is extremely difficult, a great deal of work has been done both analytically and numerically. Andersson [10] presented and compared momentum integral approaches developed by several investigators utilizing sinusoidal and polynomial velocity profile assumptions as applied to planar films. Most of these investigators assumed fully viscous film flow and neglected the boundary layer region, a region near the inlet where viscous effects have not yet fully engulfed the entire film thickness. Flow development depends upon the manner in which the film is formed and Haugen [11], Jain [12], and Roy [13] all utilized the momentum integral approach to study this region. Andersson and Ytrehus [14], on the other hand, developed a Falkner–Skan solution for the boundary layer region.

The remainder of this paper will examine laser-Doppler velocimetry data obtained in smooth laminar films along with a description of experimental equipment and technique. A procedure for adapting the integral momentum equation to predicting mass and momentum transport in cylindrical coordinates will also be presented. This paper will also examine the limitations of planar film models in predicting film flow on cylindrical surfaces commonly employed in thermal and chemical devices.

† Author to whom all correspondence should be addressed.

NOMENCLATURE

C	constant in equation (9)
g	gravitational acceleration
g^*	gravitational term defined in equation (3)
G_1	dimensionless parameter defined in equation (22)
G_2	dimensionless parameter defined in equation (26)
G_3	dimensionless parameter defined in equation (27)
$\dot{m}$	total film mass flow rate
n	constant in equation (9)
P	static pressure
r	radial distance measured from column axis
Re	film Reynolds number
R_0	dimensionless parameter defined in equation (30)
r_0	outer radius of column
r_δ	radius corresponding to free interface
u	x-direction velocity component
u'	fluctuation in x-direction velocity component
u_δ	x-direction velocity component of free interface
u_*	shear velocity, $\sqrt{(\nu[\partial u/\partial y]_{y=0})}$
v	r-direction velocity component
v'	fluctuation in r-direction velocity component
v_δ	r-direction velocity component of free interface
X	dimensionless coordinate defined in equation (31)
x	stream-wise coordinate
x_0	stream-wise position of needle contact probe
y	distance perpendicular to the wall.

Greek symbols

β	dimensionless film thickness parameter defined in equation (11)
Γ	mass flow rate per unit film width for a planar film
δ	film thickness
η	dimensionless variable defined in equation (5)
μ	dynamic viscosity
ν	kinematic viscosity
ρ	liquid density
ρ_g	density of ambient gas
ψ	dimensionless variable defined in equation (6).

Subscripts

δ	film free interface
∞	asymptotic value.

2. EXPERIMENTAL APPARATUS

The experimental apparatus used in this study consisted of four major parts: flow loop, film sampling channel, LDV system, and data acquisition system.

A schematic diagram of the flow loop is shown in Fig. 1. Approximately 0.25 m^3 of the test fluid were contained in the reservoir and circulated through the system by a 7.5 hp centrifugal pump. The liquid could be pumped through a bypass line and one of two main supply lines each containing a turbine flow meter, one for high and the other for low flow rate measurement. Downstream of the flow meters, the test fluid was forced through a flow straightening chamber. This chamber contained two baffles to ensure an even flow distribution and decelerate the fluid. Following the practice of several investigators [5, 7, 15, 16], the film was formed by injection from a porous tube. The liquid flowed from the straightening chamber into the 50 mm o.d., 610 mm long porous tube which was plugged at the lower end. With a mean porosity of 100 μm, this polyethylene tube allowed the fluid to pass through to the outside with a low radial velocity. The free fall section consisted of a 50 mm o.d., 2136 mm long polypropylene tube installed immediately after the porous tube. A diffuser was installed at the end of the free fall section in order to allow reentry of the fluid into the reservoir with minimal churning or bubble formation. The entire column was held together by a long tiebolt and adjusted to a true vertical alignment with the aid of three plumbs. The heat

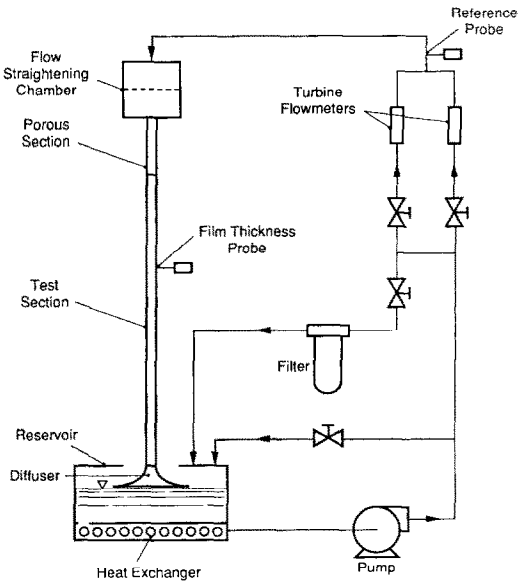

FIG. 1. Experimental flow loop.

exchanger shown in Fig. 1 was added to the system in order to eliminate the temperature rise created by pumping high viscosity fluids. An acrylic cover placed over the cooling coils forced the fluid to flow past nearly all of the coils before entering the pump. Fluid temperature was measured in two locations, the flow straightening chamber and the lower reservoir.

Since the laser light required for LDV measurements cannot be focused to a probe volume through the curved surface of the falling film, a sampling channel was constructed to slice the film. A slice of film was allowed to continue falling down the column while the rest of the film was moved out of the way of the laser beams. An isometric drawing of the sampling channel is shown in Fig. 2(a) while detailed views of the sampling channel are given in Fig. 2(b). The sampling channel walls, or splitters, were made of acrylic sheets 1.59 mm in thickness and sharpened on the outside of the leading edges. In order to allow the LDV probe volume to be located in the 'freestream' between the boundary layers formed on each splitter, they were spaced 12 mm apart. The conical access ports allowed the laser beams to pass through each splitter and be focused within the film at a location approximately 28 mm downstream of the leading edges.

The actual LDV equipment used in conjunction with the film sampling channel consisted of a TSI System 9100-7 with a 2 W Argon-ion Lexel model 95 laser, a 4 beam system minus the beam stop and field stop hardware as shown in Fig. 3. The transmitting optics included a model 9117 lens with a focal distance of approximately 121.5 mm and a model 9188-A 2.27× beam expander. These components created a very small beam crossing, 0.029 mm × 0.150 mm. Since axial velocities were high, flow reversal was not expected, and radial velocities were very low, only the line used to measure the radial component of velocity was frequency shifted. Seeding was accomplished by using air bubbles formed when the liquid reentered the tank. The configuration of the heat exchanger helped to ensure that only the smallest bubbles were entrained by the pump. The sizes of these bubbles were measured with a microscope objective, and the majority were determined to be approximately 0.01 mm in diameter. Based on calculations outlined by Adrian and Fingerson [17], air bubbles 10 times that diameter in the water/propylene glycol solutions used in the present study would follow flow fluctuations of 1000 Hz frequency with an amplitude error of less than 0.01%.

Data were collected with a Compaq 386 microcomputer interfaced with two TSI counters through a TSI model 6260 interface card and model 1998K interface module. Each record consisted of 4096 individual readings, and various data realization rates were tried with no observable effect. Data were sampled at 2000 Hz per channel and when conducting two component measurements, a 10 μs coincidence window was used.

3. OPERATING PROCEDURE

After the column was leveled with the aid of three plumbs, it was cleaned with acetone in order to remove any surface contaminants. The flow loop was allowed to operate for approximately one-half hour. This provided adequate time for thermal equilibrium to be reached and eliminated flow rate fluctuations caused by viscosity changes. The laser system was then aligned in such a way as to insure that the LDV probe

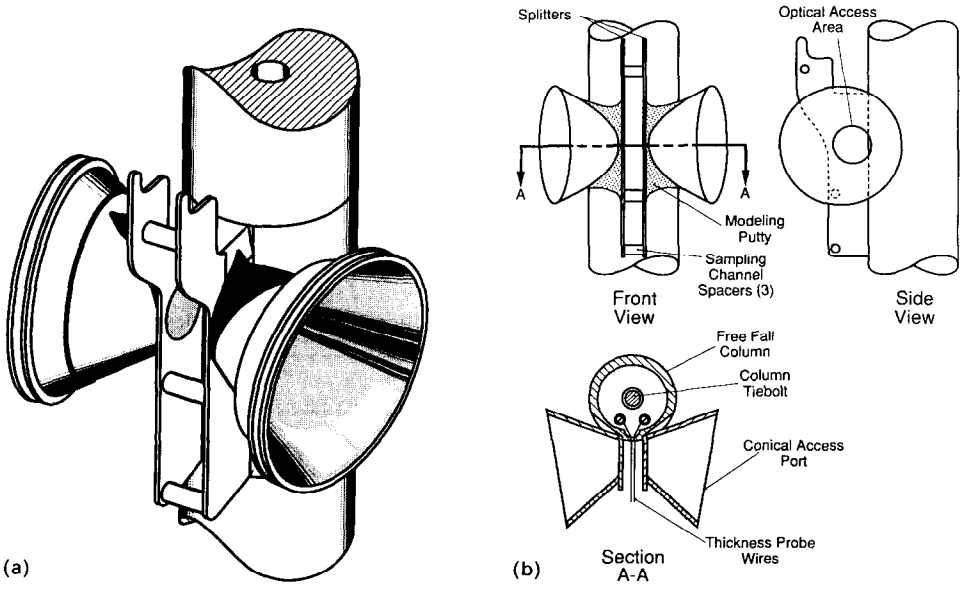

FIG. 2. Film sampling channel: (a) isometric view, (b) schematic drawing.

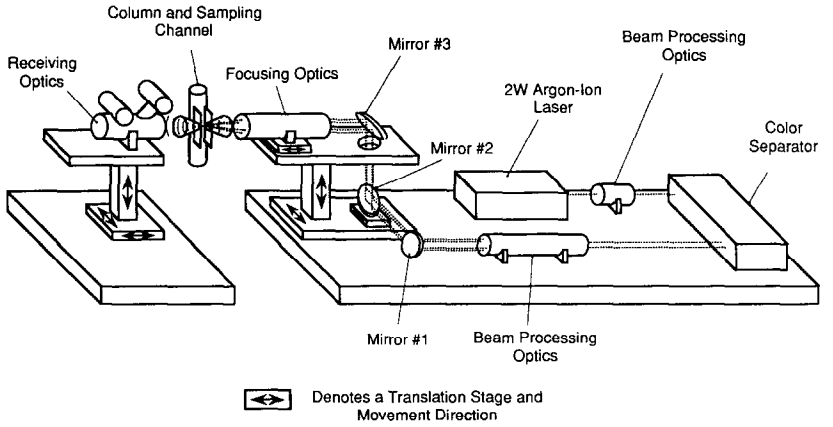

FIG. 3. Layout of LDV optical hardware.

volume traversed a radial path in the center of the sampling channel. Fortunately, the curvature of the column made it very easy to find the 'wall' and accurately position the probe volume in the film.

Since the film interface was smooth, the film thickness was determined by the position of the laser beams when they no longer entered the film. The free interfaces of these films were glass-like in appearance despite the high Reynolds numbers and made this task very straightforward. Furthermore, measured flow rates were in excellent agreement with those calculated from the measured velocity profiles, confirming the accuracy of this procedure in identifying the interface location. Wetting of the glycol solutions on the sampling channel walls was largely responsible for this success. Without wetting, interface curvature could have prevented the laser beams from reaching the outermost region of the liquid film. The geometrical error associated with this curvature would have been approximately 10% for a film thickness of 6 mm, a typical thickness obtained in the present study. Fortunately, the meniscus formed on the channel walls almost completely eliminated this problem.

Film thickness was also measured immediately below the porous tube with a needle contact probe in order to determine the upstream or 'inlet' thickness for these smooth laminar films. Since a wake was produced downstream of the needle probe when it was in contact with the liquid film and could have adversely affected the velocity measurements, the probe was not allowed to touch the film at the same time LDV data were being collected.

4. FULLY DEVELOPED LAMINAR FILM VELOCITY PROFILE

Before discussing any experimental results, it is desirable to introduce the velocity profile for a planar, fully developed, laminar, falling film. Such a film does not accelerate because viscous shear balances the gravitational body force. Nusselt [18] determined the stream-wise velocity for such a film as

$$\frac{u}{u_\delta} = 2\left[\left(\frac{y}{\delta}\right) - \frac{1}{2}\left(\frac{y}{\delta}\right)^2\right] \tag{1}$$

where u_δ is the liquid velocity at the free interface and the coordinates are as defined in Fig. 4(a). In deriving equation (1), steady flow was assumed as well as a no slip condition at the wall and negligible viscous shear at the free or air/liquid interface. This solution is sometimes referred to as the asymptotic solution.

In order to deduce the fully developed velocity distribution in the cylindrical system, Fig. 4(b), the film is assumed to be axisymmetric and the stream-wise Navier–Stokes equation reduces to

$$u\frac{\partial u}{\partial x} + v\frac{\partial u}{\partial r} = g - \frac{1}{\rho}\frac{\partial P}{\partial x} + \nu\left[\frac{\partial^2 u}{\partial x^2} + \frac{1}{r}\frac{\partial}{\partial r}\left(r\frac{\partial u}{\partial r}\right)\right]. \tag{2}$$

The wall and interfacial boundary conditions are defined as $u]_{r=r_0} = 0$ and $\partial u/\partial r]_{r=r_\delta} = 0$, respectively. Since all radial velocities and stream-wise derivatives of u are zero in a fully developed film, and the stream-wise pressure gradient is equal to the ambient pressure gradient, $\partial P/\partial x = \rho_g g$, equation (2) can be simplified as

$$-\frac{g(\rho-\rho_g)}{\rho} = \nu\left[\frac{1}{r}\frac{\mathrm{d}}{\mathrm{d}r}\left(r\frac{\mathrm{d}u}{\mathrm{d}r}\right)\right]. \tag{3}$$

Denoting the term on the left by g^*, the fully developed velocity profile can be obtained by integrating equation (3) from r to r_δ followed by a second integration from r_0 to r.

$$u = \frac{g^*}{\nu}\frac{r_\delta^2}{2}\left[\ln\left(\frac{r}{r_0}\right) - \frac{1}{2}\left(\frac{r^2-r_0^2}{r_\delta^2}\right)\right]. \tag{4}$$

If the dimensionless variables η and ψ are defined as

$$\eta \equiv \frac{r^2-r_0^2}{r_\delta^2-r_0^2} \tag{5}$$

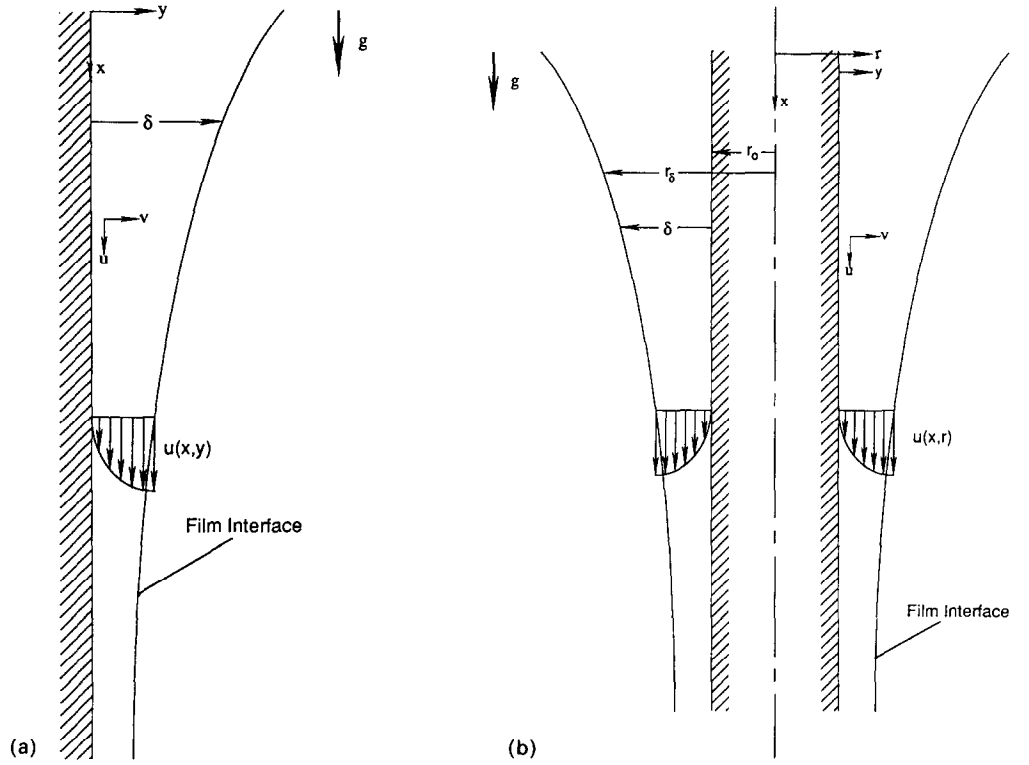

FIG. 4. Coordinates and geometry of falling liquid films: (a) planar film, (b) axisymmetric film.

$$\psi \equiv \frac{r_\delta^2 - r_0^2}{r_0^2} \tag{6}$$

then equation (4) can be expressed as

$$u = \frac{g^*}{\nu}\frac{r_0^2}{4}[(\psi+1)\ln(\eta\psi+1) - \eta\psi]. \tag{7}$$

Finally, nondimensionalizing the velocity distribution by the liquid velocity at the free interface yields the following profile:

$$\frac{u}{u_\delta} = \frac{[(\psi+1)\ln(\eta\psi+1) - \eta\psi]}{[(\psi+1)\ln(\psi+1) - \psi]}. \tag{8}$$

As can be seen, η and ψ are the nondimensional terms in the cylindrical version of a fully developed velocity distribution which correspond to the term y/δ found in the Cartesian distribution, equation (1).

5. LAMINAR FILM DATA

Experimental results were obtained from laminar falling liquid films formed with 90% and 70% propylene glycol in water. The LDV measurements were made at an axial location 1842.5 mm below the porous section. Nominal values for the respective properties of the 90% and 70% glycol mixtures at 24°C are $\rho = 1031$ and 1017 kg m^{-3}, $\mu = 0.02587$ and 0.01565 kg m^{-1} s^{-1}, and $\sigma = 0.03742$ and 0.03949 N m^{-1}.

Film thickness

Since the general form of film thickness correlation is

$$\delta\left[\frac{\rho(\rho-\rho_g)g}{\mu^2}\right]^{1/3} = C\,Re^n \tag{9}$$

the large viscosities of the propylene glycol mixtures allowed very thick films to be formed at relatively low Reynolds numbers. For example, laminar films 6 mm thick were produced at a Reynolds number of 4000 using the 90% glycol mixture. Such thicknesses allowed more than enough room for the laser beams to enter the film and form a measuring volume. Figure 5 illustrates the results of these measurements. As can be seen, the profiles, measured with a mean error of ±0.5%, were parabolic in appearance and demonstrated little evidence of significant shear at the air/liquid interface. Additionally, the differences between velocity distributions measured in 70% and 90% glycol solutions reveal the effects of viscosity.

When equation (4) is integrated from r_0 to $r_{\delta\infty}$, the asymptotic value of r_δ, an equation for volume flow rate is produced which can be rearranged to yield the following expression for Reynolds number:

$$\left(\tfrac{3}{4}Re\right)^{1/3} = \left\{\frac{\frac{3}{4}\frac{r_{\delta\infty}^4}{r_0}\left[\ln\left(\frac{r_{\delta\infty}}{r_0}\right) - \frac{1}{4}\left(3 + \frac{r_0^4}{r_{\delta\infty}^4}\right) + \frac{r_0^2}{r_{\delta\infty}^2}\right]}{(r_{\delta\infty}-r_0)^3}\right\}^{1/3} \delta_\infty \frac{(g^*)^{1/3}}{\nu^{2/3}}. \tag{10}$$

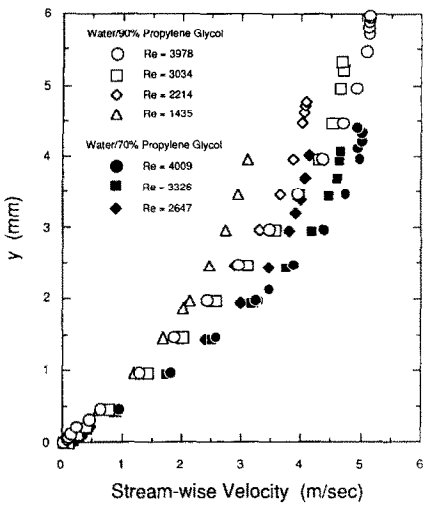

FIG. 5. Velocity profiles in laminar films.

Equation (10) was obtained from fully developed conditions, however, it can be used to define the dimensionless parameter

$$\beta \equiv \left\{ \frac{\frac{3}{4}\frac{r_{\delta\infty}^4}{r_0}\left[\ln\left(\frac{r_\delta}{r_0}\right) - \frac{1}{4}\left(3+\frac{r_0^4}{r_\delta^4}\right) + \frac{r_0^2}{r_\delta^2}\right]}{(r_\delta - r_0)^3} \right\}^{1/3} \delta \frac{(g^*)^{1/3}}{\nu^{2/3}} \tag{11}$$

where the asymptotic value of β is given by equation (10). It should be noted that as r_0 increases towards infinity, the term in brackets reduces to unity, and equation (11) becomes identical to the expression obtained by Nusselt [18] for planar films. As demonstrated by Fig. 6, the experimentally determined values of β were slightly larger than the values corresponding to fully developed flow in all cases, indicating that each film was still accelerating moderately at the measurement location.

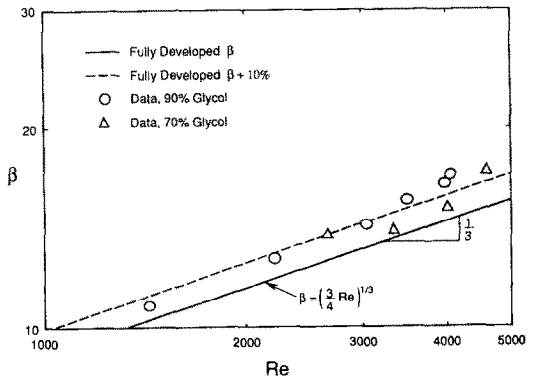

FIG. 6. Nondimensional film thickness vs Reynolds number for fully developed and developing films.

Film velocity profile

Figure 7(a) compares the nondimensionalized profiles with a fully developed profile and a profile of the form

$$\frac{u}{u_\delta} = \sin\left[\frac{\pi}{2}\frac{y}{\delta}\right]. \tag{12}$$

As shown, almost every case had a velocity profile which was only slightly different from the asymptotic or nonaccelerating profile. Equation (12) was chosen by Stücheli and Özisik [19] as a means of modeling planar films and is fairly accurate in fitting the present data. Figure 7(b) demonstrates the general agreement between the present study and the work of previous investigators who studied planar films. It is notable that the film thicknesses measured by the previous investigators, Cook and Clark [5] and Semena and Mel'nichuk [7], were a full order of magnitude less than those of the glycol films since they utilized water as the working fluid and lower Reynolds numbers. Like the present study, they employed porous sections to form liquid films. Finally, Fig. 7(c) shows the present data plotted in terms of the dimensionless variables η and u/u_δ as suggested by equation (8). A fully developed profile as well as a profile of the form

$$\frac{u}{u_\delta} = \sin\left[\frac{\pi}{2}\eta\right] \tag{13}$$

are included for comparison.

Effects of vertical misalignment

During preliminary tests, it was observed that integrating the experimentally determined velocity profile over the column circumference yielded a volume flow rate significantly different from that measured by the turbine flow meter. This discrepancy was subsequently determined to be caused by vertical misalignment of the column. Figure 8 compares velocity profiles measured in a falling liquid film formed on the outside of a vertical column and a column slightly out of vertical. The nonvertical column was out of alignment by only 0.136 degrees. Calculating the flow rate from the velocity profile corresponding to the nonvertical case yielded 4.5×10^{-3} m^3 s^{-1} (72 g.p.m.) as compared to a measured flow rate of 3.5×10^{-3} m^3 s^{-1} (55 g.p.m.). For all data presented, including those of Fig. 7, agreement between the volume flow rate computed from velocity profile integration and the measured flow rate was better than 5%.

In order to determine whether the sampling channel splitters had any effect on the previously discussed measurements, two surveys were made within the channel using 70% glycol at a Reynolds number of 4997 and 90% glycol at a Reynolds number of 1252. Since boundary layers tend to thicken with increases in viscosity and decreases in velocity, these conditions represented opposite extremes. For the water/70% propylene glycol mixture, the boundary layers formed on the sampling channel walls were less than 1.5 mm

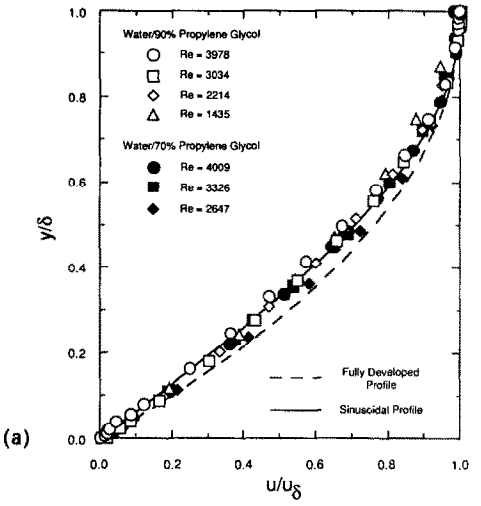

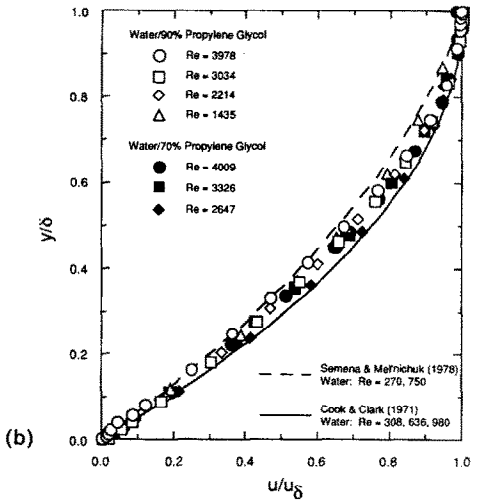

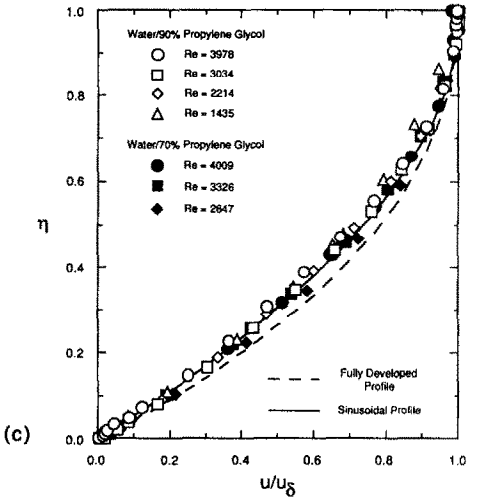

FIG. 7. Velocity profiles: (a) present data nondimensionalized in Cartesian coordinates, (b) comparison with previous planar film work, and (c) data nondimensionalized in cylindrical coordinates.

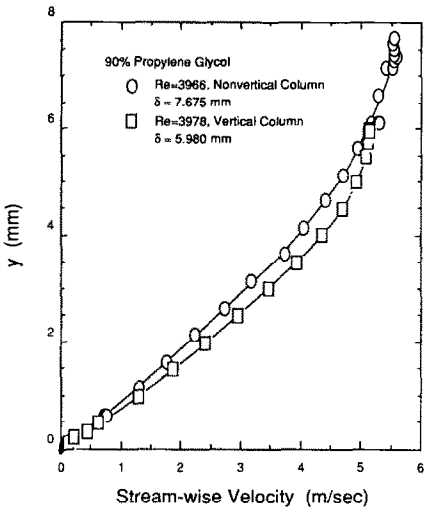

FIG. 8. Effects of vertical misalignment.

thick while they were less than 2.5 mm thick for the 90% glycol solution. The small mass deficit created by these boundary layers was actually beneficial since the liquid which would have been in the space occupied by the boundary layers crept out along the channel walls. This allowed the LDV probe volume to be moved extremely close to the air/liquid interface despite the interface's curvature.

Turbulence effects

As pointed out previously, Cook and Clark reported water films at Reynolds numbers up to 1000 as being free of waves and exhibiting parabolic velocity distributions. It was also mentioned that falling liquid films should undergo transition from laminar to wavy laminar flow at a Reynolds number of 33 and become fully turbulent beyond a Reynolds number of 1600. Since every case studied in the present investigation was neither turbulent nor wavy laminar, each case represented an exception to these general guidelines. Two component LDV measurements were conducted as a result of these observations in order to quantitatively prove that these films were laminar, as their appearance suggested. The turbulence induced shear proved to be extremely small ($\overline{u'v'}/u_*^2 < 0.02$) across the entire film thickness at Reynolds numbers well above 1600 for both the 70% and 90% propylene glycol solutions. Calculated turbulence intensities for the 90% glycol mixture were nearly constant at 1.6% for stream-wise velocity and 0.67% for the radial component. Similar results were obtained from the 70% glycol solution with 1.8% corresponding to the stream-wise velocity and 0.80% corresponding to the radial component. Additionally, neither high noise levels in the laboratory nor applying a sixteenth-inch thick layer of masking tape to the top of the free fall section could 'trip' the film into a turbulent or wavy state. Holding the volume flow rate constant while

forcing the viscosity to decrease through an increase in glycol temperature did, however, destabilize a film originally corresponding a Reynolds number of 1435 into a wavy mode. It can be postulated that the suppression of turbulence at high Reynolds numbers may be related to the effects of increased thickness, especially with the more viscous fluids, on turbulent bursts occurring at the wall. Such bursts must be dampened both by the relatively large distance from the free interface (as compared to thinner water films) and the resistance offered by the viscous forces across the film. This hypothesis is supported by the observation that smooth films were formed at high *Re* values while thinner, low *Re* and low viscosity films were marred by waviness. However, it should be emphasized that the films tested in the present study could ultimately turn wavy and turbulent had the test column been much longer, as indicated by Cook and Clark [5].

Referring to the introduction, it is interesting to note that most of the investigators who reported laminar films at unusually high Reynolds numbers formed falling liquid films with either a porous section or something closely resembling a porous section. In light of the present results, it seems likely that both viscosity and the method of film formation can significantly influence the downstream hydrodynamic behavior of a falling liquid film.

6. MODELING OF FILM DEVELOPMENT IN CYLINDRICAL COORDINATES

Since the falling liquid films presented in the previous section were not fully developed and could not be described by the asymptotic equations outlined in Section 4, a model for developing films is desired.

The continuity and stream-wise boundary layer equations for incompressible flow in cylindrical coordinates are given by the following equations:

$$\frac{\partial u}{\partial x}+\frac{1}{r}\frac{\partial (rv)}{\partial r}=0 \tag{14}$$

$$u\frac{\partial u}{\partial x}+v\frac{\partial u}{\partial r}=g-\frac{1}{\rho}\frac{\partial P}{\partial x}+\nu\left[\frac{1}{r}\frac{\partial}{\partial r}\left(r\frac{\partial u}{\partial r}\right)\right]. \tag{15}$$

With the aid of the Liebnitz Rule, the continuity equation can be integrated from r_0 to r_δ. This yields

$$v_\delta = u_\delta \frac{\mathrm{d}r_\delta}{\mathrm{d}x}. \tag{16}$$

Setting the stream-wise pressure gradient equal to the ambient pressure gradient and substituting equation (14) into (15) gives

$$u\frac{\partial u}{\partial x}+v\frac{\partial u}{\partial r}+u\left[\frac{\partial u}{\partial x}+\frac{1}{r}\frac{\partial (rv)}{\partial r}\right] = \frac{g(\rho-\rho_g)}{\rho}+\nu\left[\frac{1}{r}\frac{\partial}{\partial r}\left(r\frac{\partial u}{\partial r}\right)\right]. \tag{17}$$

By replacing the first term on the right side with g^* and simplifying the left side, equation (17) becomes

$$\frac{\partial u^2}{\partial x}+\frac{1}{r}\frac{\partial (ruw)}{\partial r}=g^*+\nu\left[\frac{1}{r}\frac{\partial}{\partial r}\left(r\frac{\partial u}{\partial r}\right)\right]. \tag{18}$$

The final form of the integral momentum equation is arrived at by integrating both sides from r_0 to r_δ, noting that the shear at the free interface is negligible, and substituting equation (16) into the result.

$$\frac{\mathrm{d}}{\mathrm{d}x}\int_{r_0}^{r_\delta} u^2 r\,\mathrm{d}r=\frac{g^*}{2}(r_\delta^2-r_0^2)-\nu r_0\left[\frac{\partial u}{\partial r}\right]_{r=r_0}. \tag{19}$$

Solving the above integral momentum equation is facilitated by assuming that the profile is preserved throughout the developing region. Using equation (8) as a guide, the velocity profile is assumed to follow the general form

$$\frac{u}{u_\delta}=f(\eta,\psi). \tag{20}$$

The mass flow rate, $\dot{m}$, can then be solved for in terms of the assumed profile.

$$\frac{\dot{m}}{\rho}=\int_{r_0}^{r_\delta} u2\pi r\,\mathrm{d}r=u_\delta \pi r_0^2\psi\int_0^1 f\,\mathrm{d}\eta=u_\delta\pi r_0^2\psi G_1 \tag{21}$$

where

$$G_1(\psi)\equiv\int_0^1 f\,\mathrm{d}\eta. \tag{22}$$

Equation (21) yields an expression relating mass flow rate, film thickness, and liquid velocity at the free interface,

$$u_\delta=\frac{\dot{m}/\rho}{\pi r_0^2\psi G_1}. \tag{23}$$

Using the assumed form of the velocity profile once again, equation (20), expressions for both the momentum flux and viscous shear terms can also be derived,

$$\frac{\mathrm{d}}{\mathrm{d}x}\int_{r_0}^{r_\delta} u^2 r\,\mathrm{d}r=\frac{\mathrm{d}}{\mathrm{d}x}\left[\tfrac{1}{2}u_\delta^2 r_0^2\psi\int_0^1 f^2\,\mathrm{d}\eta\right] = \tfrac{1}{2}r_0^2\frac{\mathrm{d}}{\mathrm{d}x}[u_\delta^2\psi G_2] \tag{24}$$

$$\nu r_0\left[\frac{\partial u}{\partial r}\right]_{r=r_0}=2u_\delta\nu\frac{1}{\psi}\left[\frac{\partial f}{\partial\eta}\right]_{\eta=0}=2u_\delta\nu\frac{1}{\psi}G_3 \tag{25}$$

where

$$G_2(\psi)\equiv\int_0^1 f^2\,\mathrm{d}\eta \tag{26}$$

$$G_3(\psi)\equiv\left[\frac{\partial f}{\partial\eta}\right]_{\eta=0}. \tag{27}$$

Equations (23)–(25) can then be substituted into the cylindrical form of the integral momentum equation

to arrive at the following differential equation:

$$\tfrac{1}{2}r_0^2\frac{\mathrm{d}}{\mathrm{d}x}\left[\left(\frac{\dot{m}/\rho}{\pi r_0^2\psi G_1}\right)^2\psi G_2\right] = \frac{g^*}{2}r_0^2\psi - 2\left(\frac{\dot{m}/\rho}{\pi r_0^2\psi G_1}\right)\nu\frac{1}{\psi}G_3. \quad (28)$$

Finally, by introducing the definition of Reynolds number, nondimensional radius, and nondimensional stream-wise distance,

$$Re \equiv \frac{4}{\mu}\left(\frac{\dot{m}}{2\pi r_0}\right) \equiv \frac{4\Gamma}{\mu} \quad (29)$$

$$R_0 \equiv r_0\frac{(g^*)^{1/3}}{\nu^{2/3}} \quad (30)$$

$$X \equiv x\frac{(g^*)^{1/3}}{\nu^{2/3}} \quad (31)$$

equation (28) can be rearranged to yield the more useful form

$$\mathrm{d}X = \frac{\left(\frac{Re}{2R_0}\right)^2\frac{1}{\psi}}{1-\frac{2\,Re}{(R_0)^3}\frac{G_3}{G_1}\frac{1}{\psi^3}}\mathrm{d}\left(\frac{G_2}{G_1^2}\frac{1}{\psi}\right) \quad (32)$$

which can be numerically integrated for any profile defined by equation (20). The asymptotic film thickness is obtained by setting the denominator of equation (32) equal to zero.

$$\psi_\infty = \left[\frac{2\,Re}{(R_0)^3}\frac{G_3(\psi_\infty)}{G_1(\psi_\infty)}\right]^{1/3}. \quad (33)$$

While any reasonable velocity profile can be assumed and used in the integral momentum approach, using equation (8) in the developing region results in the correct asymptotic film thickness and velocity profile eventually being reached. Using equation (8) to evaluate G_1, G_2, and G_3 yields the following results:

$$G_1 = \frac{\psi+1}{\psi} - \frac{\frac{\psi}{2}}{(\psi+1)\ln(\psi+1)-\psi} \quad (34)$$

$$G_2 = \frac{\left\{\frac{(\psi+1)^2}{\psi}[(\psi+1)\ln^2(\psi+1)-2(\psi+1)\ln(\psi+1)+2\psi]-\psi(\psi+1)\left[\left(1-\frac{1}{\psi^2}\right)\ln(\psi+1)+\frac{1}{\psi}-\frac{1}{2}\right]+\frac{\psi^2}{3}\right\}}{[(\psi+1)\ln(\psi+1)-\psi]^2} \quad (35)$$

$$G_3 = \frac{\psi^2}{(\psi+1)\ln(\psi+1)-\psi}. \quad (36)$$

Developing velocity profile

Predicted velocities at the measurement location, 1842.5 mm below the porous section, are shown in Figs. 9(a) and (b). As illustrated, this model predicts conditions which are somewhat more developed than the data for either 90% or 70% glycol solutions. Even in the worst case, however, the film thickness and interfacial liquid velocity are within 8.7% and 12.5% of the measured values, respectively.

Development of film thickness

Since the hydrodynamic characteristics are different for developing and fully developed flows, it is desirable to know how far a liquid film must travel before it becomes fully developed. Using the model to compute nondimensional stream-wise lengths as a function of ψ/ψ_∞ results in Figs. 10(a) and (b). In these plots, the dimensionless stream-wise length is based upon the distance from the needle contact probe, $x-x_0$. The model illustrates rapid initial change in film thickness followed by a gradual decrease to the asymptotic value. As outlined in Section 1, several investigators have modeled the boundary layer region of planar films formed from an initially uniform velocity profile. In order to gain insight into the effects caused by possible boundary layer regions existing in the present study, the model developed by Haugen [11] for planar films was applied to conditions of the present study. For 90% glycol at $Re = 1248$, a best case scenario, including the boundary layer region in calculations yielded no difference when compared to calculations ignoring such a region. For 70% glycol at $Re = 4584$, a worst case scenario, the predicted film thickness was only 2% greater when the boundary layer region was included. Furthermore, since the theoretical velocity profile formed at the base of a porous tube with an inviscid liquid can be shown to be parabolic, it is rather unlikely that a significant boundary layer region exists for a viscous fluid and that ignoring it in an integral analysis introduces any significant error.

A comparison of the model with actual data is found in Figs. 11(a) and (b). Here the ratio of ψ to ψ_∞ and the initial condition based on measurement of δ_0, ψ_0/ψ_∞, are plotted as a function of the Reynolds number. As shown, the model slightly underpredicts the measured values which indicate that the films were not quite fully developed. The odd data point in Fig. 11(b), corresponding to a Reynolds number of 2647, was due to the film being on the verge of transforming to a wavy state. This condition made determination of the actual film thickness difficult without use of a film thickness probe.

Development length

Figure 12 compares two different development length criteria by looking at the ratio of development length to stream-wise location. In the first case, the film is considered fully developed when the film thick-

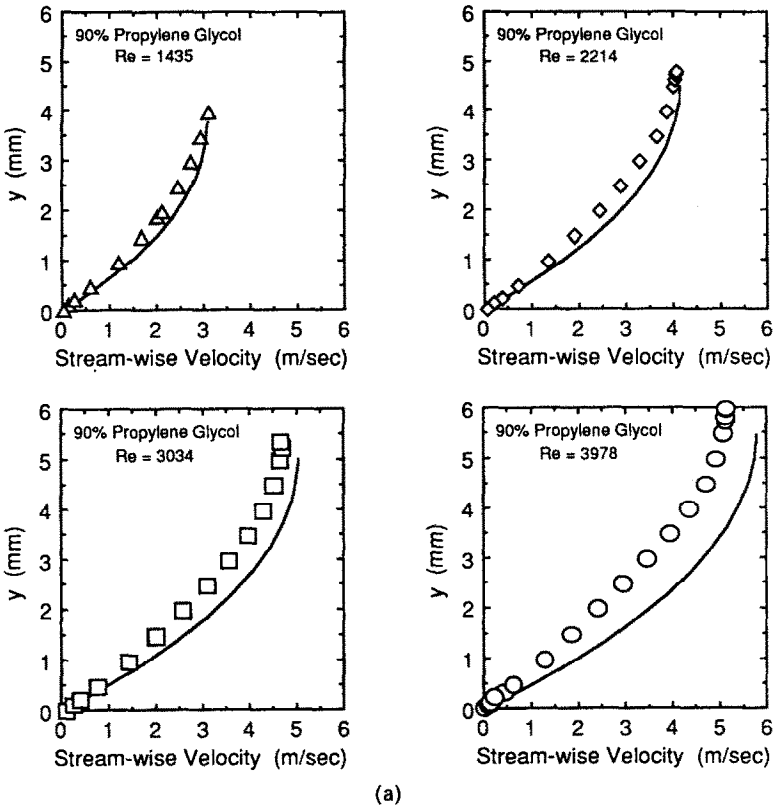

(a)

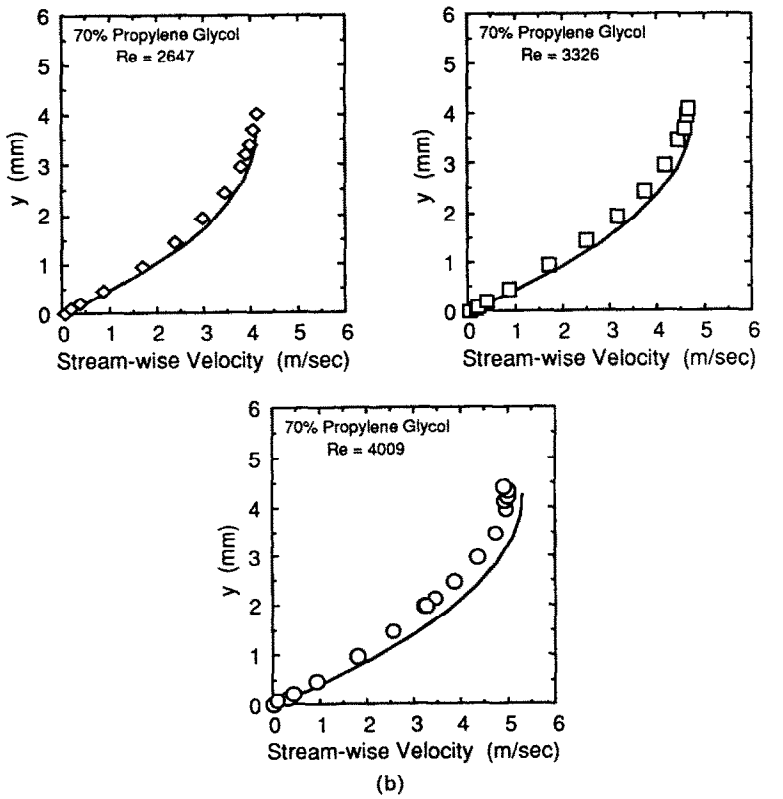

(b)

FIG. 9. Comparison of measured and predicted velocities for: (a) 90% glycol films, (b) 70% glycol films.

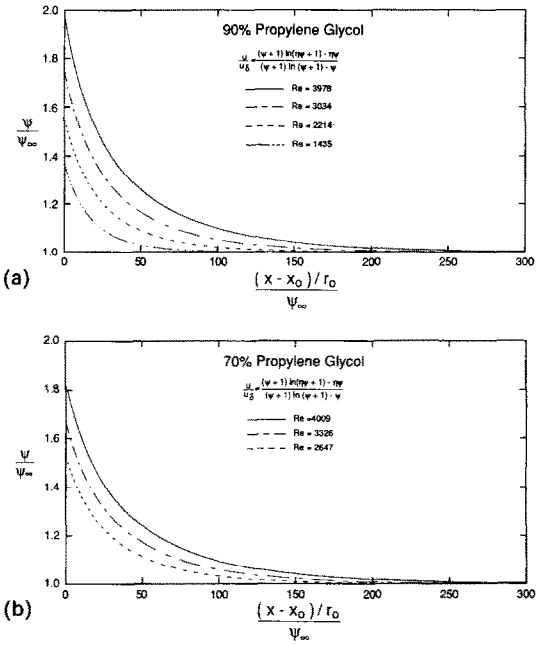

FIG. 10. Predicted development lengths for: (a) 90% glycol, (b) 70% glycol.

ness falls within 0.5% of the asymptotic value. The second case illustrates the results when the film thickness is required to fall within 5%. As shown, the development length is approximately halved by the small increase in film thickness and also increases with both Reynolds number and viscosity. Figure 12 also indicates that all of the present data satisfy the 5% criterion but some of the high Reynolds number conditions, especially those for the 90% glycol mixture, fail to satisfy the 0.5% criterion.

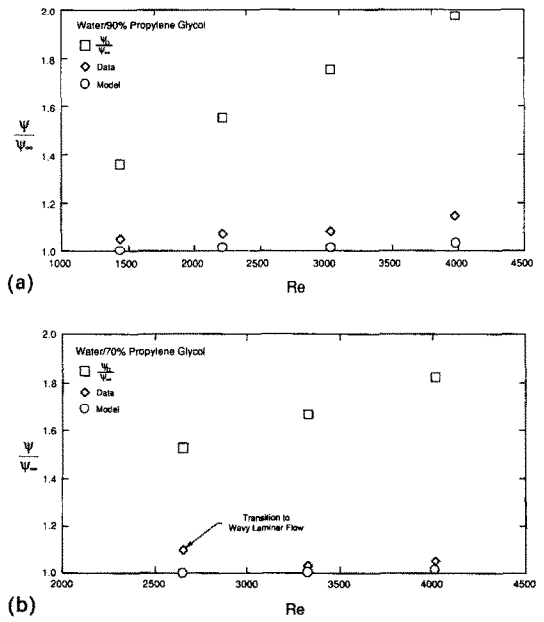

FIG. 11. ψ/ψ_∞ vs Re for: (a) 90% glycol, (b) 70% glycol.

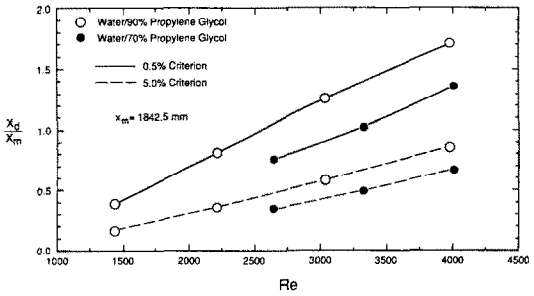

FIG. 12. Comparison of development length criteria.

Although not utilized in this paper, a closed form solution can be obtained in cylindrical coordinates if the velocity profile is assumed to a function of only η. For such a profile, equation (13) is an example, equation (32) reduces to

$$d\left(\frac{x}{r_0\psi_\infty}\right)=\frac{Re}{8}\frac{G_2}{G_1G_3}\left[\frac{d\left(\frac{\psi}{\psi_\infty}\right)}{1-\left(\frac{\psi}{\psi_\infty}\right)^3}\right] \tag{37}$$

which can be integrated to yield

$$\frac{x-x_0}{r_0\psi_\infty}=\frac{Re}{8}\frac{G_2}{G_1G_3}\left\{\tfrac{1}{6}\ln\left|\frac{1-\left(\frac{\psi}{\psi_\infty}\right)^3}{\left(\frac{\psi}{\psi_\infty}-1\right)^3}\right|+\frac{1}{\sqrt{3}}\arctan\left[\frac{\frac{2\psi}{\psi_\infty}+1}{\sqrt{3}}\right]\right\}_{\psi=\psi_0}^{\psi=\psi}. \tag{38}$$

It is also interesting to note that as r_0 is allowed to grow towards infinity, equation (32) reduces to a form given by Andersson [20] in Cartesian coordinates for some velocity profile assumptions,

$$d\left(\frac{x}{\delta_\infty}\right)=\frac{Re}{4}\frac{G_2}{G_1G_3}\left[\frac{d\left(\frac{\delta}{\delta_\infty}\right)}{1-\left(\frac{\delta}{\delta_\infty}\right)^3}\right]. \tag{39}$$

Andersson also integrated equation (39) to yield a closed form expression very similar to equation (38). Since the present cylindrical model is very easy to use, it is recommended for modeling all cylindrical situations. In light of the fact that the Cartesian velocity distribution overpredicts the fully developed interfacial liquid velocity by 5% when the ratio of film thickness to column radius reaches 8%, the cylindrical model is certainly recommended for all larger ratios.

7. SUMMARY

1. Single component LDV measurements were successfully obtained in smooth laminar films over a Reynolds number range of 1252 to 4058 in a water/90% propylene glycol solution and a range of 2647 to 4997 in a water/70% propylene glycol solution. These measurements revealed that the films were still accelerating moderately at a distance of 1842.5 mm below the porous forming section.

2. Two component velocity measurements verified that these relatively high Reynolds number films were indeed smooth laminar despite being well beyond the generally accepted range for such a flow regime. A dependence on the method of film formation was pointed out as well as a possible dependence on viscosity. It is postulated that the suppression of turbulence at high Reynolds numbers is the result of the dampening effects of increased thickness and increased viscosity on turbulent bursts occurring at the wall.

3. The velocity measurements revealed a high sensitivity of velocity profile as well as film thickness to vertical alignment of the free fall section.

4. The integral momentum equation was adapted to cylindrical coordinates and was shown to include two relevant nondimensional parameters. Streamwise velocities predicted with the integral momentum analysis were, in light of its ease of use, very close to the experimentally determined profiles. The cylindrical model is recommended over the Cartesian model for film thickness to column radius ratios exceeding 8%.

REFERENCES

1. W. M. Rohsenow, J. P. Hartnett and E. N. Ganic, *Handbook of Heat Transfer Fundamentals* (2nd Edn). McGraw-Hill, New York (1985).
2. J. O. Wilkes and R. M. Nedderman, The measurement of velocities in thin films of liquid, *Chem. Engng Sci.* **17,** 177–186 (1962).
3. S. Portalski, Velocities in film flow of liquids on vertical plates, *Chem. Engng Sci.* **19,** 575–582 (1964).
4. F. C. K. Ho and R. L. Hummel, Average velocity distributions within falling liquid films, *Chem. Engng Sci.* **25,** 1225–1237 (1970).
5. R. A. Cook and R. H. Clark, The experimental determination of velocity profiles in smooth falling liquid films, *Can. J. Chem. Engng* **49,** 412–416 (1971).
6. V. E. Nakoryakov, B. G. Pokusaev, S. V. Alekseenko and V. V. Orlov, Instantaneous velocity profile in a wavy fluid film (English translation), *J. Engng Phys.* **33,** 1012–1016 (1977).
7. M. G. Semena and G. A. Mel'nichuk, Mean-velocity distributions in a falling film, *Fluid Mech.—Sov. Res.* **7,** 145–151 (1978).
8. B. Levich, *Physicochemical Hydrodynamics.* Prentice-Hall, Englewood Cliffs (1962).
9. G. D. Fulford, The flow of liquids in thin films, *Adv. Chem. Engng* **5,** 151–236 (1964).
10. H. I. Andersson, Numerical solutions of a TSL-model for free-surface flows, *Proc. of the 5th GAMM Conf. on Numerical Methods in Fluid Mechanics*, pp. 6–16 (1984).
11. R. Haugen, Laminar flow along a vertical wall, *J. Appl. Mech.* **35,** 631–633 (1968).
12. N. C. Jain, A numerical study of the laminar flow along a vertical wall, *Acta Technica CSAV* **23,** 549–556 (1978).
13. T. R. Roy, On laminar thin-film flow along a vertical wall, *J. Appl. Mech.* **51,** 691–692 (1984).
14. H. I. Andersson and T. Ytrehus, Falkner–Skan solution for gravity-driven film flow, *J. Appl. Mech.* **52,** 783–786 (1985).
15. J. A. Shmerler and I. Mudawar, Local heat transfer coefficient in wavy free-falling turbulent liquid films undergoing uniform sensible heating, *Int. J. Heat Mass Transfer* **31,** 67–77 (1988).
16. T. H. Lyu and I. Mudawar, Statistical investigation of the relationship between interfacial waviness and heat transfer to a falling liquid film, *Int. J. Heat Mass Transfer* **34,** 1451–1464 (1991).
17. R. J. Adrian and L. M. Fingerson, Laser velocimetry theory, application, and techniques, *TSI Short Course on Laser Doppler Velocimetry*, St. Paul, MN (1987).
18. W. Nusselt, Die Oberflächenkondensation des Wasserdampfes, *Z. Ver. Deut. Ing.* **60,** 541–546, 569–575 (1916).
19. A. Stücheli and M. N. Özisik, Hydrodynamic entrance lengths of laminar falling films, *Chem. Engng Sci.* **31,** 369–372 (1976).
20. H. I. Andersson, The momentum integral approach to laminar thin-film flow, *Symposium on Thin Fluid Films, The 1987 ASME Applied Mechanics, Bioengineering, and Fluids Engineering Conf.*, Cincinnati, Ohio (1987).